



## Design, synthesis and applications of fluoride probe based on aromatization of isoquinolinium salts

Yun-Hui Zhao<sup>a,\*</sup>, Yajun Yu<sup>a</sup>, Tao Guo<sup>b,\*\*</sup>, Zhihua Zhou<sup>c</sup>, Zilong Tang<sup>a</sup>, Li Tian<sup>d,\*\*\*</sup>

<sup>a</sup> School of Chemistry and Chemical Engineering, Hunan University of Science and Technology, Xiangtan, Hunan, 411201, PR China

<sup>b</sup> School of Chemistry and Chemical Engineering, Henan University of Technology, Zhengzhou, Henan, 450001, PR China

<sup>c</sup> Hunan Provincial Key Laboratory of Controllable Preparation and Functional Application of Fine Polymers, Hunan University of Science and Technology, Xiangtan, PR China

<sup>d</sup> School of Materials Science and Engineering, Hunan University of Science and Technology, Xiangtan, PR China

### ARTICLE INFO

#### Keywords:

Isoquinolinium salts  
Fluoride determination  
Ratiometric chemosensor  
Aromatization

### ABSTRACT

A novel ratiometric fluorescent probe based on aromatization drive of isoquinolinium salts was designed, synthesized to recognize fluoride. The applications have shown that the probe has high selectivity and sensitivity to fluoride. Fluoride induces a cascade reaction of hydroxyl deprotection and 1,6-oxidative elimination, and causes a remarkable fluorescence enhancement. The relative fluorescent intensities ( $I_{398}/I_{522}$ ) increased linearly with  $F^-$  concentration in the range of 0–9.0  $\mu\text{mol L}^{-1}$ . The limit of detection was very low (3.7 nM) due to the intrinsic aromatization drive of probe induced by  $F^-$ . The recognition mechanism was demonstrated by mass spectrum (MS) and  $^1\text{H}$  NMR. The *in vitro* imaging results showed that the new probe **BIQS** (2-[4-(*tert*-butyl-diphenylsilyloxy)-benzyl]-3-(4-methoxy-phenyl)-isoquinolinium nitrate) was membrane-permeable and could be applied into the determination of fluoride ions in living cells.

### 1. Introduction

With the rapid development of fluorescent analytical sensing and optical imaging, fluorescent probes based on organic dyes have become important tools in the research of biological and medical fields because of their high sensitivity and technical simplicity. The fluorescent signal of chemosensors will be inhibited or enhanced during the interaction with the target species by quenching off or removing quenching effects. Fluorescent probes are commonly used in many areas such as analytical chemistry, biochemistry, medicine and environmental monitoring because of the real-time and on-line detection or monitoring of target objects with the help of changes in fluorescent signals [1–5]. The fluorescent probes are roughly divided into three types: fluorescence quenching, fluorescence enhancement and ratiometric probes. The first two types provide only a single emission feature, and it may be difficult to quantify the target analyte due to the interference from various analyte-independent factors, such as instrument parameters, the microenvironment surrounding the probe molecule, and the local concentration of the probe [6–10]. To conquer this limitation, the

ratiometric fluorescent probes that harvest the target-induced fluorescent intensity changes from two different emission bands were explored. Most importantly, the ratiometric fluorescent sensing characteristic improves signal-to-noise ratios and enhances accuracy for much reliable quantification of specific analytes.

Fluoride is one of the important trace elements which play crucial roles in human body and is an indispensable component of teeth and bones [11,12]. The proper amount of fluoride in body not only makes the bone hard, but also benefits the uptake of calcium and phosphorus to consolidate the formation of bone [13,14]. Therefore, fluoride ion is often observed in toothpaste and in pharmaceutical agents as an essential ingredient. On the other hand, over deposition of fluoride in human body would lead to dental and skeletal fluorosis, which can cause severe toxicity to the biological tissue and even lead to many serious neurodegenerative diseases [15–18]. For example, in cell biology system, an excessive absorption of sodium fluoride can affect a number of essential cellular signal transduction processes and obstruct normal cellular metabolism [19]. In view of the importance of its homeostasis in physiology, tremendous effort has been devoted to the development of

\* Corresponding author.

\*\* Corresponding author.

\*\*\* Corresponding author.

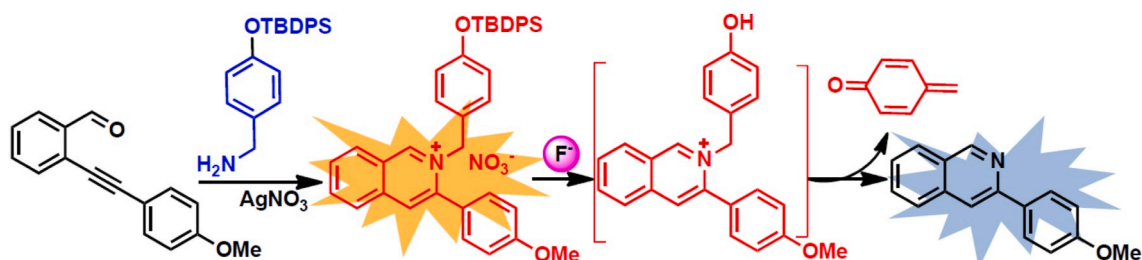
E-mail address: [zhao\\_yunhui@163.com](mailto:zhao_yunhui@163.com) (Y.-H. Zhao).

<https://doi.org/10.1016/j.dyepig.2020.108547>

Received 16 April 2020; Received in revised form 10 May 2020; Accepted 12 May 2020

Available online 18 May 2020

0143-7208/© 2020 Elsevier Ltd. All rights reserved.



Scheme 1. Possible mechanism of isoquinolinium salt for fluoride detection.

highly selective and sensitive chemosensors for the detection of fluoride, in biological systems, even in living animals. Among the reported methods, such as ion selective electrodes (ISE) [20–22], high performance liquid chromatography (HPLC) [23,24], spectrophotometry [25], ion chromatography [26,27], fluorimetry and fluorescent probes [28–32], fluorescence sensing is a powerful method for recognition of fluoride in biological systems, even in living animals due to its superiorities of high sensitivity and selectivity, simple operation, low cost.

In recent years, several types of fluorescent probes for recognition of fluoride were performed by different reaction mechanisms, e.g. the formation of hydrogen bonds between NH and fluoride ion, the complexation of boron-fluoride, and the desilylation reaction by fluoride [33–37]. However, there are some drawbacks associated with existing sensing methods. For example, the “turn-on” fluorescent anion chemosensors for selective fluoride determination often require complicated preparation procedures [38–40]. In addition, the addition of cetyl trimethyl ammonium bromide (CTAB) was necessary to increase the rate of desilylation in aqueous solution for some probes [41]. In order to address the solubility in aqueous solution, several cationic probes were designed and exhibited excellent selectivity and sensitivity for fluoride [42,43]. These studies further indicated that the *N*-alkylated cationic probes have the potential ability to target mitochondria of living cells. Isoquinoline derivatives are nitrogen-containing compounds with good fluorescence emission [44,45]. Due to the “push-pull”  $\pi$ -electron system, isoquinolinium salts have better fluorescence emission than isoquinolines. If a isoquinoline is combined with a reactive site to form a fluorescent probe isoquinolinium salt for ratio sensing and imaging of anions, the probe will release the leaving group and restore to the parent structure isoquinoline in the presence of the target detection analyte. Methylene benzoquinone is a very good leaving molecule via oxidative elimination because of the stable electronic structure [46–49]. In this work, we developed a novel fluorescent probe which takes advantage of a fluoride-induced hydroxyl deprotection and aromatization of isoquinolinium salt for the detection of fluoride (Scheme 1). The probe has three advantages: detecting fluoride in aqueous solution without the addition of CTAB; high detection sensitivity due to the intramolecular aromatization; offering visual detection of fluoride on paper strip.

## 2. Experimental

### 2.1. Chemicals and instrumentation

*Ortho*-alkynylarylaldehydes were synthesized according to Ref. [50–54] Benzylamine (98%) and silver nitrate (99%) were purchased from Guoyao Chemical Reagent Co. (Shanghai). All other normal reagents and solvents were of analytical-reagent grade and used directly without further purification. Deionized water was employed throughout the whole detection procedure. The stock solution of  $1.0 \times 10^{-3}$  mol L<sup>-1</sup> fluoride ion was prepared by dissolving 26.1 mg of Bu<sub>4</sub>NF in 100 ml deionized water. Stock solutions of other control anions were obtained by dissolving appropriate amounts of their soluble sodium salts in deionized water.

### 2.2. Synthesis of benzyl isoquinolinium salts

General procedure: AgNO<sub>3</sub> (0.5 mmol, 85 mg) was added to the solution of 2-(arylethynyl)benzaldehyde (0.5 mmol) and benzylamine (0.50 mmol, 1.0 equiv) in 1,2-dichloroethane (DCE, 3 ml). Then, the reaction mixture was stirred at 80 °C for 12 h. After been cooled to room temperature, H<sub>2</sub>O (5 ml) was added to the mixture. The mixture was extracted with DCM (3 × 10 ml). The combined extracts were washed with brine and dried over anhydrous Na<sub>2</sub>SO<sub>4</sub>, filtered, and the solvent evaporated to dryness. The crude residue was subjected to silica gel (200–300 mesh) chromatography eluted with DCM/MeOH (20:1, v/v) to afford the desired products. All synthesized dyes were fully characterized and confirmed by <sup>1</sup>H NMR, <sup>13</sup>C NMR, IR and HRMS spectroscopy (see supporting information Figs. S1–S27).

2-Benzyl-3-(4-methoxy-phenyl)-isoquinolinium nitrate (**3a**), pale yellow solid, M.p 94–97 °C. IR (KBr) cm<sup>-1</sup> 3431, 2924, 2853, 2421, 2049, 2025, 1639, 1608, 1504, 1458, 1380, 1251, 1180, 1093, 1021, 905, 840, 765, 716, 695, 575, 540, 512, 473. <sup>1</sup>H NMR (500 MHz, CDCl<sub>3</sub>)  $\delta$  10.769 (s, 1H), 8.615 (d, *J* = 8.0 Hz, 1H), 8.025 (t, *J* = 7.5 Hz, 1H), 7.959–7.936 (m, 2H), 7.828 (t, *J* = 7.5 Hz, 1H), 7.227–7.186 (m, 2H), 7.159–7.101 (m, 3H), 6.945 (d, *J* = 8.0 Hz, 2H), 6.839 (d, *J* = 7.5 Hz, 2H), 5.976 (s, 2H), 3.820 (3.820, 3H). HRMS calcd for C<sub>23</sub>H<sub>20</sub>NO [M]<sup>+</sup> 326.1539, found 326.1539.

2-Benzyl-3-*p*-tolyl-isoquinolinium nitrate (**3b**), yellow oily liquid, IR (KBr) cm<sup>-1</sup> 3432, 2923, 2853, 2048, 2025, 1635, 1500, 1383, 573, 515. <sup>1</sup>H NMR (500 MHz, CDCl<sub>3</sub>)  $\delta$  10.786 (s, 1H), 8.633 (d, *J* = 8.0 Hz, 1H), 8.043 (t, *J* = 7.5 Hz, 1H), 7.990–7.963 (m, 2H), 7.840 (t, *J* = 7.5 Hz, 1H), 7.259 (d, *J* = 8 Hz, 2H), 7.198–7.152 (m, 3H), 7.117 (t, *J* = 7.5 Hz, 2H), 6.847 (d, *J* = 7.5 Hz, 2H), 5.980 (s, 2H), 2.399 (s, 3H). <sup>13</sup>C NMR (125 MHz, CDCl<sub>3</sub>)  $\delta$  153.2, 146.2, 141.4, 137.8, 137.7, 133.5, 131.8, 131.2, 129.9, 129.7, 129.1, 129.1, 128.9, 128.2, 127.5, 127.3, 126.6, 62.1, 21.5. HRMS calcd for C<sub>23</sub>H<sub>20</sub>N [M]<sup>+</sup> 310.1590, found 310.1590.

2-Benzyl-3-phenyl-isoquinolinium nitrate (**3c**), yellow oily liquid. IR (KBr) cm<sup>-1</sup> 3432, 2921, 2845, 2048, 2025, 1715, 1635, 1381, 1227, 572. <sup>1</sup>H NMR (500 MHz, CDCl<sub>3</sub>)  $\delta$  10.822 (s, 1H), 8.648 (d, *J* = 7 Hz, 1H), 8.059 (t, *J* = 7.5 Hz, 1H), 8.005–7.983 (m, 2H), 7.854 (t, *J* = 7.5 Hz, 1H), 7.521 (t, *J* = 7.5 Hz, 1H), 7.441 (t, *J* = 7.5 Hz, 2H), 7.301 (d, *J* = 7.5 Hz, 2H), 7.157 (t, *J* = 7.5 Hz, 1H), 7.100 (t, *J* = 7.5 Hz, 2H), 6.797 (d, *J* = 7.5 Hz, 2H), 5.978 (s, 2H). <sup>13</sup>C NMR (125 MHz, CDCl<sub>3</sub>)  $\delta$  153.3, 145.9, 137.8, 137.7, 133.3, 131.8, 131.8, 131.3, 130.9, 129.8, 129.2, 129.1, 129.1, 128.2, 127.5, 127.4, 126.7, 62.3. HRMS calcd for C<sub>22</sub>H<sub>18</sub>N [M]<sup>+</sup> 296.1434, found 296.1433.

2-Benzyl-3-(4-chloro-phenyl)-isoquinolinium (**3d**), yellow oily liquid. IR (KBr) cm<sup>-1</sup> 3432, 2924, 2026, 1711, 1638, 1605, 1491, 1359, 1088, 839, 763. <sup>1</sup>H NMR (400 MHz, CDCl<sub>3</sub>)  $\delta$  10.63 (s, 1H), 8.58 (d, *J* = 8.4 Hz, 1H), 8.05–8.04 (m, 3H), 7.85–7.81 (m, 1H), 7.41 (d, *J* = 8.4 Hz, 2H), 7.31 (d, *J* = 8.4 Hz, 2H), 7.20–7.11 (m, 3H), 6.79 (d, *J* = 7.2 Hz, 2H), 5.94 (s, 2H). <sup>13</sup>C NMR (100 MHz, CDCl<sub>3</sub>)  $\delta$  153.1, 144.7, 137.8, 137.7, 137.2, 133.1, 131.6, 131.4, 131.3, 130.2, 129.4, 129.1, 128.8, 128.1, 127.7, 127.4, 126.9, 62.6. HRMS calcd for C<sub>22</sub>H<sub>17</sub>ClN [M]<sup>+</sup> 330.1044, found 330.1043.

2-Benzyl-3-(4-chloro-phenyl)-7-methyl-isoquinolinium nitrate (**3e**), yellow solid. M.p 173–175 °C. IR (KBr) cm<sup>-1</sup> 3434, 3033, 2960, 2920,

2851, 2049, 2025, 1636, 1612, 1497, 1454, 1376, 1198, 1088, 1015, 853, 831, 765, 736, 703, 560, 558, 511, 474.  $^1\text{H}$  NMR (500 MHz,  $\text{CDCl}_3$ )  $\delta$  10.574 (s, 1H), 8.335 (s, 1H), 7.918–7.879 (m, 3H), 7.387 (d,  $J = 8$  Hz, 2H), 7.264 (d,  $J = 8$  Hz, 2H), 7.168 (t,  $J = 7.5$  Hz, 1H), 7.115 (t,  $J = 7.5$  Hz, 2H), 6.786 (d,  $J = 7.5$  Hz, 2H), 5.938 (s, 2H), 2.543 (s, 3H).  $^{13}\text{C}$  NMR (125 MHz,  $\text{CDCl}_3$ )  $\delta$  152.5, 144.0, 142.6, 140.2, 137.2, 136.0, 133.3, 131.3, 130.3, 130.1, 129.4, 129.2, 128.1, 127.8, 127.2, 126.5, 62.1, 21.9. HRMS calcd for  $\text{C}_{23}\text{H}_{19}\text{ClN}$   $[\text{M}]^+$  344.1201, found 344.1200.

2-Benzyl-7-chloro-3-(4-chloro-phenyl)-isoquinolinium nitrate (3f), yellow solid. M.p 161–164 °C. IR (KBr)  $\text{cm}^{-1}$  3417, 3061, 3030, 2924, 2854, 2054, 2026, 1643, 1602, 1516, 1490, 1451, 1379, 1189, 1082, 1022, 1000, 929, 833, 724, 697, 672, 602, 578, 511, 474.  $^1\text{H}$  NMR (500 MHz,  $\text{CDCl}_3$ )  $\delta$  10.744 (s, 1H), 8.520 (s, 1H), 8.016–7.969 (m, 2H), 7.882 (d,  $J = 8.5$ , 1H), 7.368 (d,  $J = 8.5$  Hz), 7.306 (d,  $J = 8.5$  Hz, 2H), 7.158 (t,  $J = 7.5$  Hz, 1H), 7.097 (t,  $J = 7.5$  Hz, 2H), 6.773 (d,  $J = 7.5$  Hz, 2H), 5.949 (s, 2H).  $^{13}\text{C}$  NMR (125 MHz,  $\text{CDCl}_3$ )  $\delta$  152.5, 145.2, 138.4, 137.6, 137.4, 136.1, 132.9, 131.3, 130.0, 129.7, 129.4, 129.3, 129.2, 128.6, 128.2, 128.2, 127.5, 62.9. LCMS calcd for  $\text{C}_{22}\text{H}_{16}\text{Cl}_2\text{N}$   $[\text{M}]^+$  364.0, found 363.9. HRMS calcd for  $\text{C}_{22}\text{H}_{16}\text{Cl}_2\text{N}$   $[\text{M}]^+$  364.0654, found 364.0653.

2-Benzyl-7-chloro-3-phenyl-isoquinolinium nitrate (3g), yellow solid, M.p 89–91 °C. IR (KBr)  $\text{cm}^{-1}$  3430, 3050, 3016, 2920, 2851, 2049, 2025, 1638, 1598, 1515, 1492, 1451, 1383, 1188, 1102, 1078, 930, 907, 833, 765, 729, 701, 601, 571, 510, 479.  $^1\text{H}$  NMR (500 MHz,  $\text{CDCl}_3$ )  $\delta$  10.897 (s, 1H), 8.588 (s, 1H), 8.022–7.989 (m, 2H), 7.921 (dd,  $J = 1.5$  Hz, 8.5 Hz, 1H), 7.514 (t,  $J = 7.5$  Hz, 1H), 7.432 (t,  $J = 7.5$  Hz, 2H), 7.325 (d,  $J = 7.5$  Hz, 2H), 7.152 (t,  $J = 7.5$  Hz, 1H), 7.089 (t,  $J = 7.5$  Hz, 2H), 6.800 (d,  $J = 7.5$  Hz, 2H), 5.997 (s, 2H).  $^{13}\text{C}$  NMR (125 MHz,  $\text{CDCl}_3$ )  $\delta$  152.5, 146.4, 138.5, 137.5, 136.2, 133.0, 131.6, 131.0, 129.8, 129.3, 129.2, 129.1, 128.5, 128.3, 128.2, 127.4, 62.6. HRMS calcd for  $\text{C}_{22}\text{H}_{17}\text{ClN}$   $[\text{M}]^+$  330.1044, found 330.1043.

2-Benzyl-7-methoxy-3-phenyl-isoquinolinium nitrate (3h), pale yellow solid, M.p 98–101 °C. IR (KBr)  $\text{cm}^{-1}$  3430, 3055, 3008, 2923, 2853, 2051, 2026, 1614, 1498, 1452, 1382, 1216, 1180, 1106, 1021, 937, 838, 763, 613, 566, 514.  $^1\text{H}$  NMR (500 MHz,  $\text{CDCl}_3$ )  $\delta$  10.717 (s, 1H), 8.014 (s, 1H), 7.878–7.852 (m, 2H), 7.650 (dd,  $J = 2$  Hz, 9 Hz, 1H), 7.512 (t,  $J = 7.5$  Hz, 1H), 7.432 (t,  $J = 7.5$  Hz, 2H), 7.267 (d,  $J = 7.5$  Hz, 2H), 7.155 (t,  $J = 7.5$  Hz, 1H), 7.099 (t,  $J = 7.5$  Hz, 2H), 6.797 (d,  $J = 7.5$  Hz, 2H), 5.926 (s, 2H), 3.966 (s, 3H).  $^{13}\text{C}$  NMR (125 MHz,  $\text{CDCl}_3$ )  $\delta$  161.4, 150.9, 143.8, 133.4, 131.6, 130.8, 129.9, 129.2, 129.1, 129.1, 128.1, 127.9, 126.9, 107.9, 62.2, 56.6. LCMS calcd for  $\text{C}_{23}\text{H}_{20}\text{NO}$   $[\text{M}]^+$  326.1, found 326.0. HRMS calcd for  $\text{C}_{23}\text{H}_{20}\text{NO}$   $[\text{M}]^+$  326.1539, found 326.1538.

2-[4-(*Tert*-butyl-diphenyl-silyloxy)-benzyl]-3-(4-methoxy-phenyl)-isoquinolinium nitrate (BIQS), pale yellow solid, M.p 99–102 °C, IR (KBr)  $\text{cm}^{-1}$  3441, 2927, 2853, 2048, 2025, 1704, 1635, 1506, 1383, 1256, 1179, 1110, 1028, 916, 826, 703, 572.  $^1\text{H}$  NMR (500 MHz,  $\text{CDCl}_3$ )  $\delta$  10.675 (s, 1H), 8.580 (d,  $J = 7.5$  Hz, 1H), 7.999 (t,  $J = 7.5$  Hz, 1H), 7.936 (d,  $J = 8.0$  Hz, 1H), 7.880 (s, 1H), 7.804 (t,  $J = 7.5$  Hz, 1H), 7.572 (d,  $J = 7.5$  Hz, BIQS), 7.342 (t,  $J = 7.5$  Hz, 2H), 7.272 (t,  $J = 7.5$  Hz, BIQS), 7.123 (d,  $J = 8.0$  Hz, 2H), 6.842 (d,  $J = 8.0$  Hz, 2H), 6.563 (d,  $J = 8.5$  Hz, 2H), 6.510 (d,  $J = 8.0$  Hz, 2H), 5.809 (s, 2H), 3.766 (s, 3H), 0.975 (s, 9H).  $^{13}\text{C}$  NMR (125 MHz,  $\text{CDCl}_3$ )  $\delta$  161.3, 156.3, 152.9, 145.9, 137.7, 137.4, 135.4, 132.4, 131.7, 131.3, 131.1, 130.1, 129.7, 127.8, 127.4, 126.6, 125.8, 123.9, 120.3, 114.6, 62.0, 55.6, 26.4, 19.4. HRMS calcd for  $\text{C}_{39}\text{H}_{38}\text{NO}_2\text{Si}$   $[\text{M}]^+$  580.2666, found 580.2668.

### 2.3. Cell imaging

The bioimaging application of BIQS for fluoride sensing in living cells was researched. CellTiter 96® Aqueous One Solution Cell Proliferation Assay was purchased from Promega (Madison, WI, USA). Cell culture media was purchased from Thermo Scientific HyClone (MA, USA). Hela cells were cultured in Dulbecco modified eagle medium (DMEM) supplemented with 10% (v/v) heat-inactivated fetal calf serum, 100  $\mu\text{g}/\text{ml}$  penicillin, under an atmosphere of 5%  $\text{CO}_2$  at 37 °C in a humidified air. The cells were treated with BIQS and were allowed to

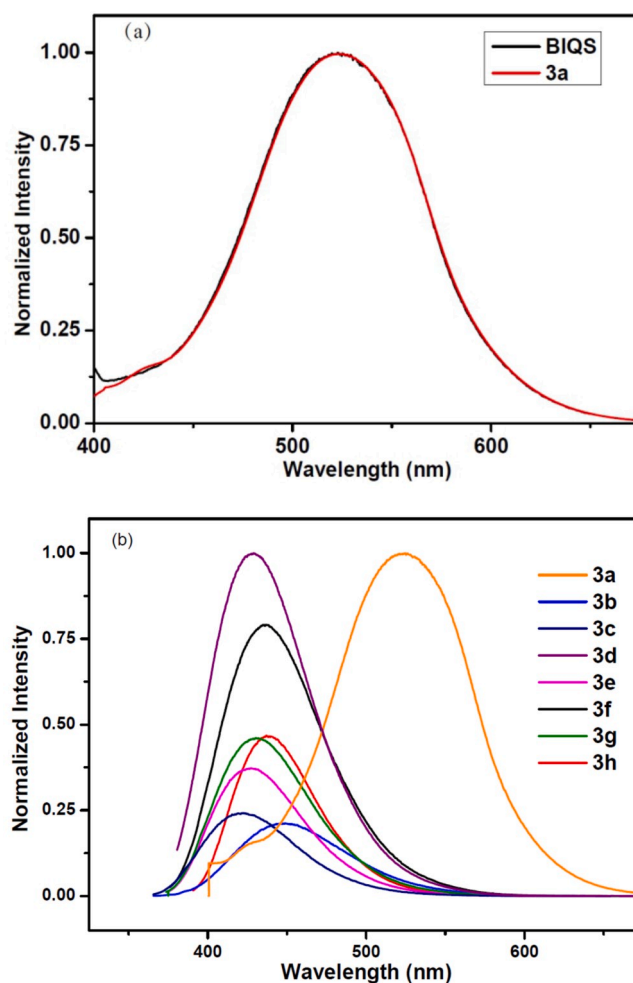
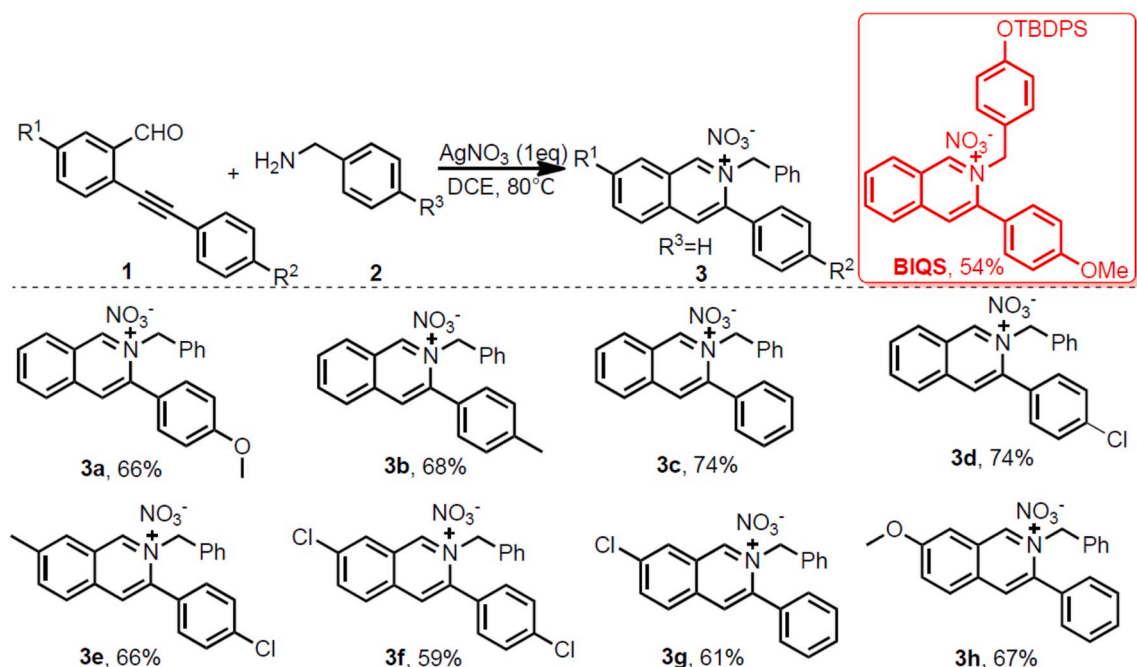


Fig. 1. (a) Fluorescent emission of compounds 3a and BIQS in MeCN. (b) Fluorescent emission of compounds 3a–3h in MeCN.

incubate at 37 °C for half an hour in 5%  $\text{CO}_2$ . Then the cells were washed with phosphate buffer saline (PBS) and new prepared fluoride solution was added. After incubation for 30 min at 37 °C and washing twice with PBS, the fluorescence images were acquired with an Olympus IX81 inverted microscope with an Olympus FV1000 confocal scanning system.

### 3. Results and discussion

The traditional method for preparing isoquinoline salt is to utilize the benzylation of isoquinoline. However, this method has the disadvantages of low yield and difficult purification. We developed a new method for preparation of benzyl isoquinolinium salts from 2-ethynylbenzaldehyde 1 and benzylamine 2. The optimal reaction conditions were obtained by screening the reaction conditions using 2-((4-methoxyphenyl) ethynyl)benzaldehyde 1a and benzylamine 2 as model substrates. The desired product 3a could be obtained in 66% yield under the presence of 100% mol  $\text{AgNO}_3$  in DCE at 80 °C. The target compound was confirmed by comparison with the known isoquinolinium salts [55] with a typical chemical shifts at 10.7 ppm. The substituents at the benzyl group  $\text{R}^3$  would have little effect on the fluorescent property of isoquinolinium salts because the conjugated structure of the dye molecular skeleton is not affected. In order to verify this assumption, the probe BIQS was synthesized under the same reaction condition. As seen from Fig. 1a, the fluorescent emission spectra of compounds 3a and BIQS were almost the same. The result confirmed the previous deduction. Consequently, a



**Scheme 2.** Different substituted isoquinolinium salts were prepared under the presence of  $\text{AgNO}_3$  in DCE.

series of isoquinolinium salts with no substituents at benzyl  $\text{R}^3$  was prepared to study their spectral property without the need to synthesize relatively complex probe molecules. We would then synthesize the target probe based on the spectral properties of these compounds. Therefore, other benzylisoquinolinium salts having different substituents at  $\text{R}^1$  and  $\text{R}^2$  were obtained under optimal reaction conditions in moderate to good yields (Scheme 2).

All isoquinolinium salts were stable under ambient conditions, and were soluble in common organic solvents, such as DCM, MeCN, EtOH and THF. The maximum absorption wavelengths of these compounds were between 350 and 380 nm (Fig. S28). To our delight, these isoquinolinium salts exhibited excellent fluorescence emission at 400–600 nm. As seen from Fig. 1b, the maximum emission wavelengths shifted from 522 to 445, 421, and 428 nm, when the substituents at  $\text{R}^2$  changed from methoxyl (**3a**) to methyl (**3b**), hydrogen (**3c**), and chlorine (**3d**), respectively. Compound **3a** showed the largest emission wavelength and highest intensity among these isoquinolinium salts because of the strongest electron-donating group methoxyl [56]. However, when the substituent at  $\text{R}^2$  was diethylamino (not show), the maximum emission peak shifted to a shorter wavelength than that of compound **3a** and the intensity was also very weak. This phenomenon may be explained by the intramolecular charge transfer due to the presence of diethylamino. On the other hand, the maximum emission wavelengths exhibited an increasing trend when the substituents at  $\text{R}^1$  changed from methyl (**3e**) to hydrogen (**3d**) and chlorine (**3f**). Based on the above results, the dye **BIQS** having the same dye moiety of **3a**, which has the best fluorescence performance among the obtained isoquinolinium salts, was chosen as the parent structure for the determination of fluoride.

A detailed study of **BIQS**'s spectral properties was conducted before the recognition of fluoride. The UV–vis spectra of **BIQS** (10  $\mu\text{M}$  in MeCN) displayed an absorption peak at 348 nm and the fluorescent spectra showed an emission peak at 522 nm (Fig. S29). In order to apply this dye to an aqueous environment, the effect of MeCN volume concentration on fluorescence properties was investigated, and the results were summarized in Fig. S30. It indicated that the fluorescence intensity enhanced gradually with the increased concentration of MeCN in mixed solution. The fluorescent emission quenching may be caused by the aggregation of probe molecule in aqueous solution. To facilitate actual sample analysis, a 90% MeCN– $\text{H}_2\text{O}$  solution was selected as the reaction

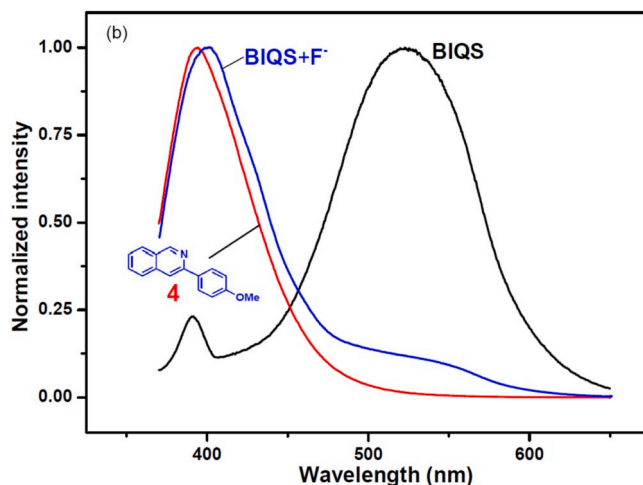


**Fig. 2.** Fluorescent emissions of **BIQS**, **4** and the mixed solution of **BIQS** and fluoride.

medium in the following experiments. The color of probe system tuned from yellow-green to colorless quickly after the addition of an equivalent fluoride. Coincidentally, the fluorescence spectrum of the probe after the addition of fluoride was very similar to that of isoquinoline **4** containing the corresponding parent structure (Fig. 2). The above results indicated that after the diphenyl-tert-butylsilyl group (TBDPS) of the dye **BIQS** was captured by fluoride, an oxidative elimination reaction was initiated by aromatization to afford the isoquinoline **4**.

Then the titration experiments were carried out *via* the addition of increasing amounts of  $\text{F}^-$  to the **BIQS** in 90% MeCN– $\text{H}_2\text{O}$  mixture. It can be seen from Fig. 3 that the emission wavelength of **BIQS** appeared at around 520 nm and the Stokes shift was about 170 nm ( $\lambda_{\text{ex}} = 350$  nm). After the addition of  $\text{F}^-$ , the peak at around 520 nm weakened gradually, and a new peak at around 400 nm began to emerge. The large shift (about 120 nm) between the two peaks would reduce the interference of background noise and increase the detection accuracy, which is a better advantage than the normal ratiometric or single signal sensors. With an

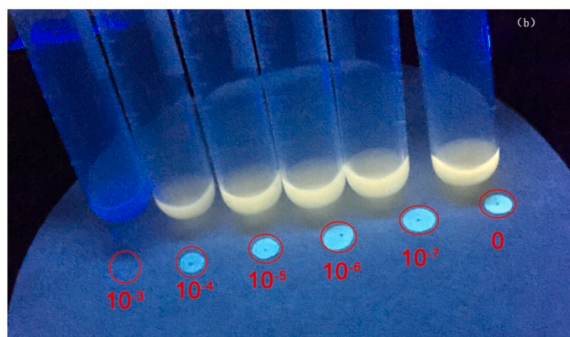
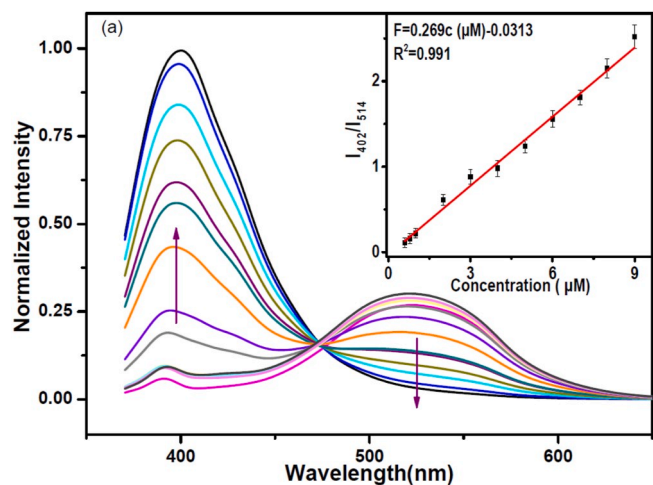


**Fig. 3.** (a) Fluorescent emission changes of **BIQS** ( $10 \mu\text{mol L}^{-1}$ ) in the presence of increasing amounts of  $\text{F}^-$  (0, 0.2, 0.4, 0.6, 0.8, 1.0, 2.0, 3.0, 4.0, 5.0, 6.0, 7.0, 8.0, 9.0,  $10 \mu\text{mol L}^{-1}$ ) in 90% MeCN–H<sub>2</sub>O (v/v) and the linear relationship between the relative fluorescent intensities ( $I_{398}/I_{522}$ ,  $F$ ) and concentration of fluoride. Incubation reactions were performed for 20 min. The fluorescence responses were obtained with 350 nm excitation and collected at 398 and 522 nm. (b) Solid-state fluorescence response of the **BIQS** with different concentrations of fluoride under UV illumination at 365 nm.

increasing amount of fluoride, the peak at around 400 nm enhanced gradually, and the peak at around 520 nm weakened accordingly. The calibration curve showed that there was an excellent linear relationship between the relative intensities ( $I_{398}/I_{522}$ ) over the fluoride concentration range of 0–9.0  $\mu\text{mol L}^{-1}$ . The linear regression equation was calculated to be  $F = 0.269c [\mu\text{mol L}^{-1}] - 0.0313$  ( $n = 11$ ,  $R^2 = 0.991$ ). The limit of detection was calculated from three times the standard deviation of the background noise to be  $3.7 \times 10^{-9} \text{ mol L}^{-1}$ . This value was much lower than the limit concentration of fluoride ( $211 \mu\text{M}$ ) in drinking water determined by the United States Environmental Protection Agency.

The sensing of fluoride on filter paper was subsequently conducted after drop-casting  $12 \mu\text{L}$  of  $1.0 \times 10^{-3} \text{ M}$  **BIQS** solution in MeCN and drying. Then, tetrabutylammonium fluoride (TBAF) solutions from  $1.0 \times 10^{-3} \text{ M}$  to  $1.0 \times 10^{-6} \text{ M}$  were added onto the stained filter paper, and pictures were recorded under ultraviolet illumination, which were shown in Fig. 3B. It was obvious that the dye **BIQS** on paper strip provided concentration-dependent fluorescence intensity decrease response to fluoride, and  $1.0 \times 10^{-3} \text{ M}$  fluoride anion could be easily identified by the naked eye because the probe molecular structure was destroyed in the presence of fluoride. This represented the dye which could provide a simple and visual method for fluoride recognition on paper strip.

The higher selectivity towards  $\text{F}^-$  compare to other potentially relevant anions is very crucial for a new fluoride sensor. For this reason, the anions response property of **BIQS** ( $10 \mu\text{M}$ ) was subsequently investigated by adding  $\text{F}^-$  and other various anions, such as  $\text{Br}^-$ ,  $\text{Cl}^-$ ,  $\text{IO}_4^-$ ,

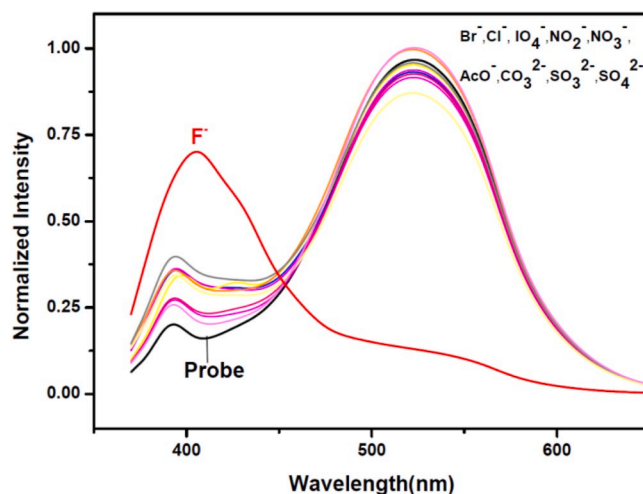


**Fig. 4.** Fluorescent emission changes of **BIQS** ( $10 \mu\text{mol L}^{-1}$ ) upon addition of various anions in 90% MeCN–H<sub>2</sub>O solution. Incubation reaction was performed for 30 min. The fluorescence responses were obtained with 350 nm excitation and collected at 398 and 522 nm.

$\text{NO}_2^-$ ,  $\text{NO}_3^-$ ,  $\text{CO}_3^{2-}$ ,  $\text{AcO}^-$ ,  $\text{SO}_3^{2-}$ ,  $\text{SO}_4^{2-}$  in  $\text{CH}_3\text{CN}/\text{H}_2\text{O} = 9/1$  (v/v). After each of these anions was added for half an hour, the fluorescence spectra of solution **BIQS** were recorded. It can be seen from Fig. 4, a small amount of  $\text{F}^-$  (0.5 equiv.) gave sharp increase in fluorescence spectra at 398 nm and drastically decrease at emission 522 nm. No obvious changes were observed upon addition of other anions even at high concentration (3 equiv.). Due to the high affinity of fluoride to silicon, the reaction-based probe **BIQS** only triggered by fluoride and undergo an oxidative-elimination process to provide isoquinoline **4**. Consequently, these results indicated that our probe has a high selectivity toward  $\text{F}^-$  ions.

In order to verify our proposed fluoride-induced deprotection group, followed by the oxidation-elimination mechanism,  $^1\text{H}$  NMR spectra was applied to monitor the dynamic process of  $\text{F}^-$  recognition with **BIQS** in  $\text{CDCl}_3$  before and after the addition of fluoride. It could be found from Fig. 5 that **BIQS** showed two sharp single peaks around 10.7 and 5.8 ppm, corresponding to the signals of the proton  $\text{N}=\text{CH}$  (benzyl isoquinolinium salts) and the protons  $\text{CH}_2\text{Ph}$  respectively. The  $^1\text{H}$  NMR signals of **BIQS** didn't change obviously under the UV illumination for 3 h in the absence of fluoride ion, which demonstrated the dye was stable in  $\text{CDCl}_3$ . After the addition of fluoride in 1 min, the signal of the  $\text{N}=\text{CH}$  was weakened dramatically and showed 1.4 ppm upfield shift, while a new peak at around 9.3 ppm emerged immediately. The new emerged peak coincided with the  $\text{N}=\text{CH}$  of isoquinoline **4** completely [50]. The phenomenon further confirmed the proposed mechanism that the probe was induced by fluoride and undergone an oxidative-elimination process to form isoquinoline immediately after the protected group been deprotected. Further evidence was confirmed by the gradually disappearance of the peak at 8.6 ppm corresponding to proton  $\text{H}^c$ . The signals of  $\text{H}^a$  and  $\text{H}^c$  were almost disappeared after 20 min. The nuclear magnetic dynamic monitoring process implies that the concentration of fluoride can be determined in a short time. The fast detection process indicated that the intrinsic aromatization drive of isoquinolinium salts was very strong.

MS was further used to confirm the desilylation process induced by fluoride. No desired peaks were observed during the deprotection process. Fortunately, the desired intermediate, hydroxybenzyl isoquinolinium salt, was found in the synthesis of isoquinoline-like reactions. The reaction between 4-hydroxybenzylamine and *o*-alkynylaldehyde catalyzed by  $\text{AgNO}_3$  produced isoquinoline **4** via a cation intermediate (corresponding to the peak 342.0). It would experience a 1,6-oxidative elimination reaction to release methylene benzoquinone

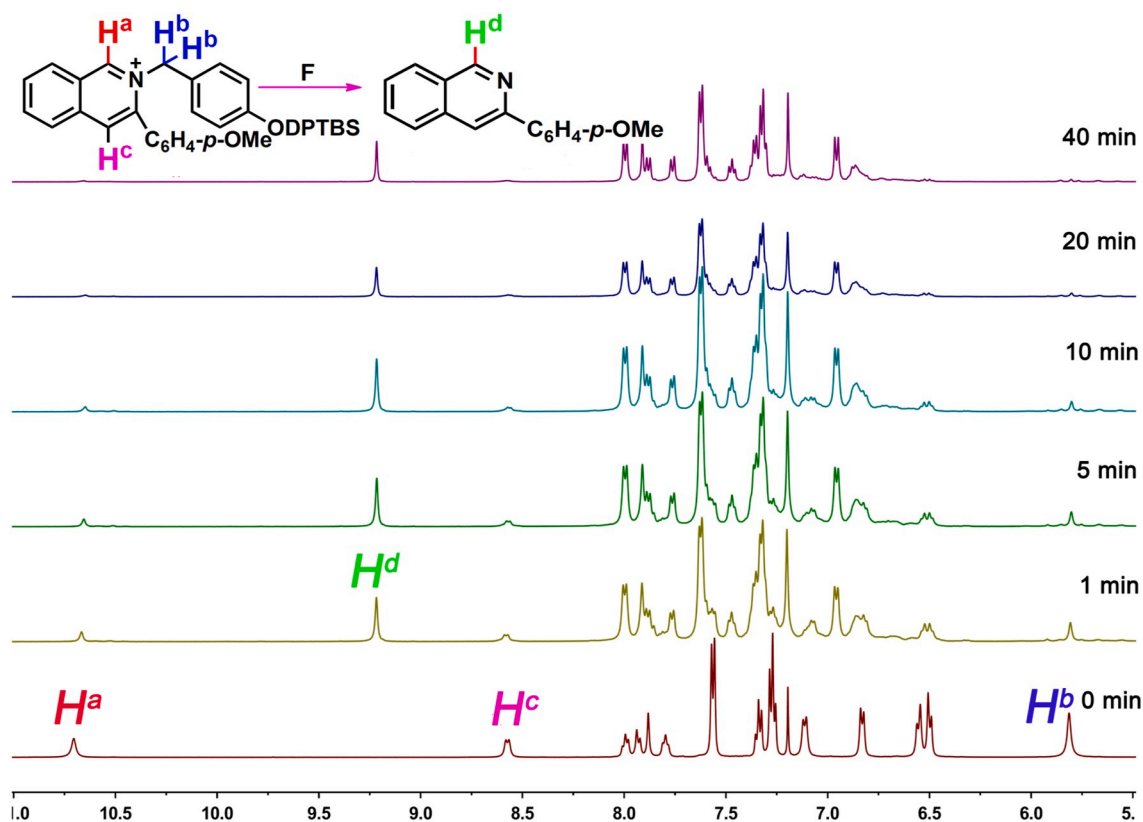


Fig. 5. The changes of  $^1\text{H}$  Chemical shift (ppm) under the presence of fluoride with increasing of reaction time.

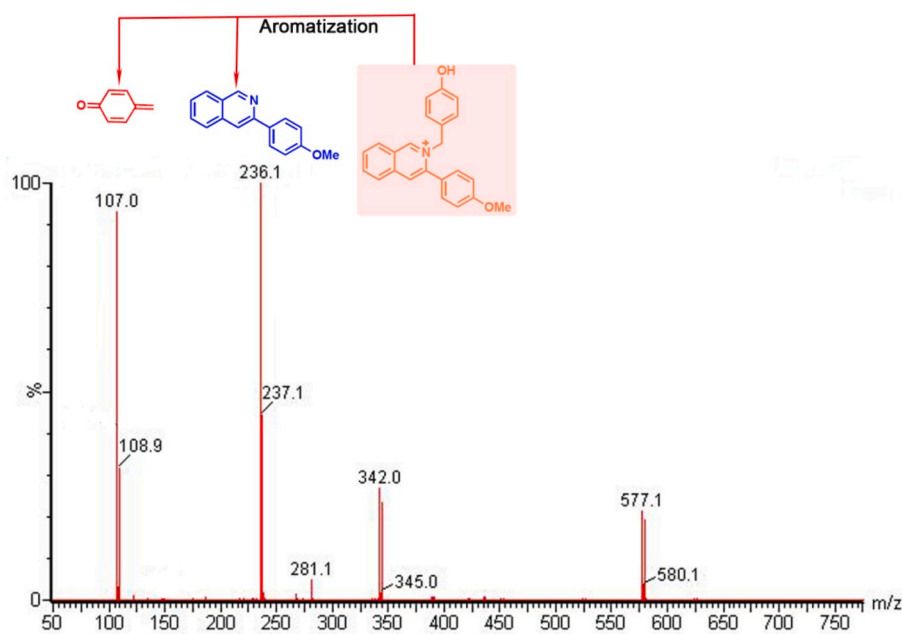
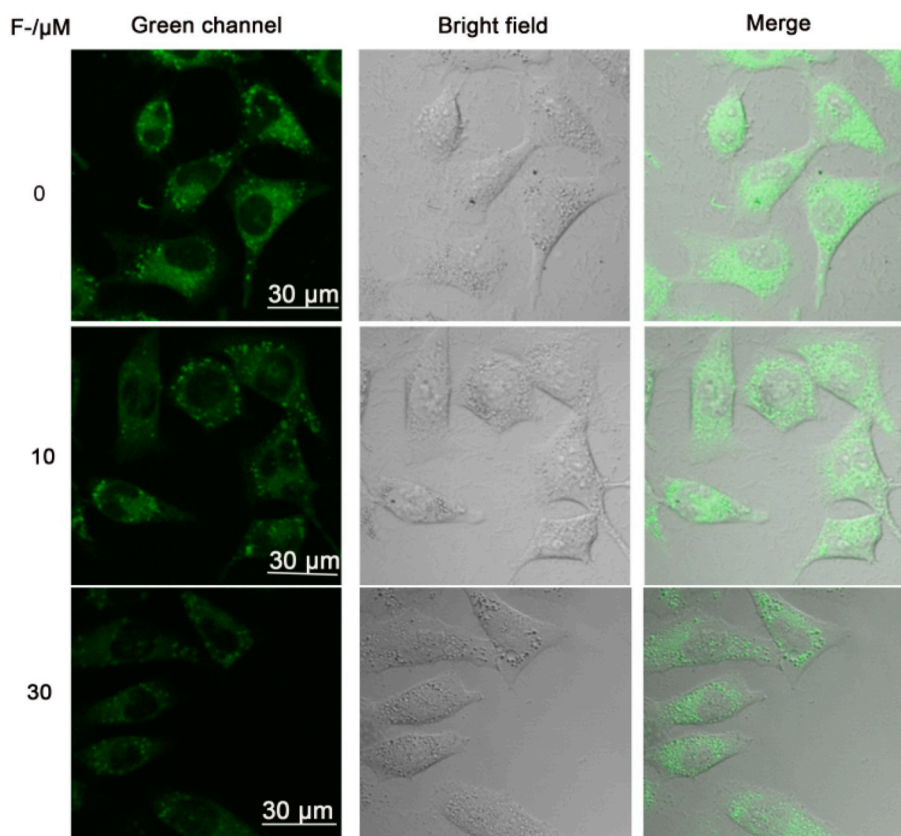


Fig. 6. The intermediates of this determination process were detected by MS.

(corresponding to the peak 107.0) and provided another fluorescent molecule isoquinoline (corresponding to the peak 236.1) because of the driving of aromatization (Fig. 6). The reaction process was completely consistent with our assumption.

Enlightened by the positive results, the fluorescence response of fluoride ion in HeLa cells using the probe BIQS was further investigated through fluorescence confocal microscopy. HeLa cells were incubated in

DMEM with BIQS (10  $\mu\text{M}$ ) for half an hour, followed by washing three times with PBS buffer. The cells were then incubated with 10 and 30  $\mu\text{M}$   $\text{F}^-$  for half an hour. Immediate visualization of fluorescence response of the probe BIQS to fluoride was carried out after been washed twice with PBS buffer. As showed in Fig. 7, the control cells displayed a strong green fluorescence after been stained with the probe BIQS. However, the cellular fluorescence intensity decreased obviously after the addition of



**Fig. 7.** Fluorescence images ( $\lambda_{\text{ex}} = 405 \text{ nm}$ ) of HeLa cells incubated with **BIQS** ( $10 \mu\text{M}$ ) for 30 min and then further incubated with fluoride ( $10, 30 \mu\text{M}$ ) for another 30 min at  $37^\circ\text{C}$ . Image of green channel (left), bright field (middle) and their composition. Scale bar =  $30 \mu\text{m}$ . (For interpretation of the references to color in this figure legend, the reader is referred to the Web version of this article.)

fluoride ion. In addition, higher concentrations of fluoride ( $30 \mu\text{M}$ ) caused more pronounced fluorescence quenching of the probe compared to lower concentrations ( $10 \mu\text{M}$ ). These results indicated that the dye **BIQS** had membrane-permeability and could be utilized to the recognition and image of fluoride in living cells.

#### 4. Conclusion

In summary, we have described the design and synthesis of a novel fluorescent probe **BIQS** for rapid and convenient recognition of fluoride. The structure-activity relationship of the substituents on the dyes was studied in detail, and it was found that the dye had the maximum fluorescence emission when the  $\text{R}^2$  position was methoxy. The probe exhibited higher fluoride selectivity over other anions, which was ascribed to the high affinity of fluoride for silicone. The detection mechanism was verified by mass spectroscopy analysis, and the dynamic detection process was further monitored by a spectrum analysis of nuclear magnetic resonance. Due to its high affinity to fluoride and aromatization drive, the probe was very sensitive to fluoride and has a very low detection limit. **BIQS** had also been successfully applied for monitoring and imaging fluoride in HeLa cells under physiological conditions.

#### Declaration of competing interest

The authors declare no conflict of interest.

#### Acknowledgements

The generous financial support from the National Natural Science Foundation of China (Nos. 51773057 and 21877034), the Hunan

Provincial Education Department Scientific Research Fund (No. 18B221) are gratefully acknowledged.

#### Appendix A. Supplementary data

Supplementary data to this article can be found online at <https://doi.org/10.1016/j.dyepig.2020.108547>.

#### References

- [1] Wang F, Wang L, Chen X, Yoon J. Recent progress in the development of fluorometric and colorimetric chemosensors for detection of cyanide ions. *Chem Soc Rev* 2014;43:4312–24.
- [2] Ding Y, Li X, Li T, Zhu W, Xie Y.  $\alpha$ -Monoacylated and  $\alpha,\alpha'$ - and  $\alpha,\beta'$ -diacylated dipyrins as highly sensitive fluorescence “turn-on”  $\text{Zn}^{2+}$  probes. *J Org Chem* 2013;78:5328–38.
- [3] Lee MH, Kim JS, Sessler JL. Small molecule-based ratiometric fluorescence probes for cations, anions, and biomolecules. *Chem Soc Rev* 2015;44:4185–91.
- [4] Liu H-W, Chen L, Xu C, Li Z, Zhang H, Zhang X-B, Tan W. Recent progresses in small-molecule enzymatic fluorescent probes for cancer imaging. *Chem Soc Rev* 2018;47:7140–80.
- [5] Li W, Gong X, Fan X, Yin S, Su D, Zhang X, Yuan L. Recent advances in molecular fluorescent probes for organic phosphate biomolecules recognition. *Chin Chem Lett* 2019;30:1775–90.
- [6] Chen X, Zhou Y, Peng X, Yoon J. Fluorescent and colorimetric probes for detection of thiols. *Chem Soc Rev* 2010;39:2120–35.
- [7] Zhou Y, Xu Z, Yoon J. Fluorescent and colorimetric chemosensors for detection of nucleotides. *Chem Soc Rev* 2011;40:2222–35.
- [8] Kim HN, Guo Z, Zhu W, Yoon J, Tian H. Recent progress on polymer-based fluorescent and colorimetric chemosensors. *Chem Soc Rev* 2011;40:79–93.
- [9] Kim HN, Ren WX, Kim JS, Yoon J. Fluorescent and colorimetric sensors for detection of lead, cadmium, and mercury ions. *Chem Soc Rev* 2012;41:3210–44.
- [10] Sun W, Guo S, Hu C, Fan J, Peng X. Recent development of chemosensors based on cyanine platforms. *Chem Rev* 2016;116:7768–817.
- [11] Matsui H, Morimoto M, Horimoto K, Nishimura Y. Some characteristics of fluoride-induced cell death in rat thymocytes: cytotoxicity of sodium fluoride. *Toxicol Vitro* 2007;21:1113–20.

- [12] Horowitz HS. The 2001 CDC recommendations for using fluoride to prevent and control dental caries in the United States. *J Publ Health Dent* 2003;63:3–8.
- [13] Kleerekoper M. The role of fluoride in the prevention of osteoporosis. *Endocrinol Metab Clin N Am* 1998;27:441–52.
- [14] Newbrun EJ. What we know and do not know about fluoride. *Public Health Dent* 2010;70:227–33.
- [15] Arhima MH, Gulati OP, Sharma SC. The effect of Pycnogenol on fluoride induced rat kidney lysosomal damage in vitro. *Phytother Res* 2004;18:244–6.
- [16] Ayoub S, Gupta AK. Fluoride in drinking water: a review on the status and stress effects. *Crit Rev Environ Sci Technol* 2006;36:433–87.
- [17] Anuradha CD, Kanno S, Hirano S. Fluoride induces apoptosis by caspase-3 activation in human leukemia HL-60 cells. *Arch Toxicol* 2000;74:226–30.
- [18] Refsnes M, Schwarze PE, Holme JA, Lag M. Fluoride-induced apoptosis in human epithelial lung cells (A549 cells): role of different G protein-linked signal systems. *Hum Exp Toxicol* 2003;22:111–23.
- [19] Barbier O, Arreola-Mendoza L, Del Razo LM. Molecular mechanisms of fluoride toxicity. *Chem Biol Interact* 2010;188:319–33.
- [20] Capka V, Bowers CP, Narvesen JN, Rossi RE. Determination of total fluorine in blood at trace concentration levels by the Wickbold decomposition method with direct potentiometric detection. *Talanta* 2004;64:869–78.
- [21] Ruiz-Payan A, Ortiz M, Duarte-Gardea M. Determination of fluoride in drinking water and in urine of adolescents living in three counties in Northern Chihuahua Mexico using a fluoride ion selective electrode. *Microchem J* 2005;1:19–22.
- [22] Hutchinson JP, Evenhuis CJ, Johns C, Kazarian AA, Breadmore MC, Macka M, Hilder EF, Guijt RM, Dicosnoski GW, Haddad PR. Identification of inorganic improvised explosive devices by analysis of postblast residues using portable capillary electrophoresis instrumentation and indirect photometric detection with a light-emitting diode. *Anal Chem* 2007;79:7005–13.
- [23] Nishimoto J, Yamada T, Tabata M. Solvent extraction and fluorometric determination of fluoride ion at ppb level in the presence of large excess of aluminum(III) and iron(III) by using an expanded porphyrin, sapphyrin. *Anal Chim Acta* 2001;428:201–8.
- [24] Garrido M, Lista AG, Palomeque M, Band BSF. Fluorimetric determination of fluoride in a flow assembly integrated on-line to an open/closed FIA system to remove interference by solid phase extraction. *Talanta* 2002;58:849–53.
- [25] Xu XR, Li HB, Gu JD, Peng KJ. Determination of fluoride in water by reversed-phase high-performance liquid chromatography using F<sup>-</sup>-La<sup>3+</sup>-alizarin complexone ternary complex. *Chromatographia* 2004;59:745–7.
- [26] Li HB, Xu XR. Separation and determination of fluoride in plant samples. *Talanta* 1999;48:57–62.
- [27] Themelis DG, Tzanavaras PD. Simultaneous spectrophotometric determination of fluoride and monofluorophosphate ions in toothpastes using a reversed flow injection manifold. *Anal Chim Acta* 2001;429:111–6.
- [28] Zhao Y-H, Li Y, Long Y, Zhou Z, Tang Z, Deng K, Zhang S. Highly selective fluorescence turn-on determination of fluoride ions via chromogenic aggregation of a silyloxy-functionalized salicylaldehyde azine. *Tetrahedron Lett* 2017;58:1351–5.
- [29] Mohapatra S, Das RK. Dopamine integrated B, N, S doped CQD nanoprobe for rapid and selective detection of fluoride ion. *Anal Chim Acta* 2019;1058:146–54.
- [30] Qi F, Zhang F, Mo L, Ren X, Wang Y, Li X, Liu X, Zhang Y, Yang Z, Song X. A HBT-based bifunctional fluorescent probe for the ratiometric detection of fluoride and sulphite in real samples. *Spectrochim Acta A* 2019;219:547–51.
- [31] Zhou Y, Zhang JF, Yoon J. Fluorescence and colorimetric chemosensors for fluoride-ion detection. *Chem Rev* 2014;114:5511–71.
- [32] Wu X, Wang H, Yang S, Tian H, Liu Y, Sun B. Highly sensitive ratiometric fluorescent paper sensors for the detection of fluoride ions. *ACS Omega* 2019;4(3):4918–26.
- [33] Han J, Zhang J, Gao M, Hao H, Xu X. Recent advances in chromo-fluorogenic probes for fluoride detection. *Dyes Pigments* 2019;162:412–39.
- [34] Zhang Y, Tu Q, Chen L, Li N, Yang L, Zhang X, Yuan M-S, Wang J. A fluorescein-based AND-logic FPSi probe for the simultaneous detection of Hg<sup>2+</sup> and F<sup>-</sup>. *Talanta* 2019;202:323–8.
- [35] Zeng L, Yuan Y, Jiang C, Mu J, Li F, Wan Y, Xu H, Qu J, Huang P, Lin J. A near-infrared turn-on probe for in vivo chemoselective photoacoustic detection of fluoride ion. *Dyes Pigments* 2019;165:408–14.
- [36] Ke B, Chen W, Ni N, Cheng Y, Dai C, Dinh H, Wang B. A fluorescent probe for rapid aqueous fluoride detection and cell imaging. *Chem Commun* 2013;49:2494–6.
- [37] Zhu B, Kan H, Liu J, Liu H, Wei Q, Du B. A highly selective ratiometric visual and red-emitting fluorescent dual-channel probe for imaging fluoride anions in living cells. *Biosens Bioelectron* 2014;52:298–303.
- [38] Selvaraj M, Rajalakshmi K, Nam Y-S, Lee Y, Song J-W, Lee H-J, Lee K-B. On-off-on relay fluorescence recognition of ferric and fluoride ions based on indicator displacement in living cells. *Anal Chim Acta* 2019;1066:112–20.
- [39] Krishnaveni K, Murugesan S, Siva A. Dual-mode recognition of biogenic amine tryptamine and fluoride ions by a naphthyl hydrazone platform: application in fluorescence imaging of HeLa cells and zebrafish embryos. *New J Chem* 2019;43:9021–31.
- [40] Zhou G, Cheng Y, Wang L, Jing X, Wang F. Novel polyphenylenes containing phenol-substituted oxadiazole moieties as fluorescent chemosensors for fluoride ion. *Macromolecules* 2005;38:2148–53.
- [41] Hu R, Feng J, Hu D, Wang S, Li S, Li Y, Yang G. A rapid aqueous fluoride ion sensor with dual output modes. *Angew Chem, Int Ed* 2010;49:4915–8.
- [42] Xu J, Sun S, Li Q, Yue Y, Li Y, Shao S. A novel “Turn-On” fluorescent probe for F<sup>-</sup> detection in aqueous solution and its application in live-cell imaging. *Anal Chim Acta* 2014;849:36–42.
- [43] Shen Y, Zhang X, Zhang Y, Li H, Chen Y. An ICT-Modulated strategy to construct colorimetric and ratiometric fluorescent sensor for mitochondria-targeted fluoride ion in cell living. *Sensor Actuator B Chem* 2018;258:544–9.
- [44] Xu J, Zhang Y, Yu H, Gao X, Shao S. Mitochondria-targeted fluorescent probe for imaging hydrogen peroxide in living cells. *Anal Chem* 2016;88:1455–61.
- [45] Tang Y, Yu Y, Wei X, Yang J, Zhu Y, Zhao Y-H, Tang Z, Zhou Z, Li X, Yu X. An efficient approach to isoquinoline via AgNO<sub>3</sub>-promoted 6-endo-dig cyclization followed by oxidative elimination of o-alkynylarylaldimines and its application in fluoride recognition. *Tetrahedron Lett* 2019. <https://doi.org/10.1016/j.tetlet.2019.151187>.
- [46] Richard JP, Amyes TL, Toteva MM. Formation and stability of carbocations and carbanions in water and intrinsic barriers to their reactions. *Acc Chem Res* 2001;34:981–8.
- [47] Richard JP, Toteva MM, Crugeiras J. Structure– reactivity relationships and intrinsic reaction barriers for nucleophile additions to a quinone methide: a strongly resonance-stabilized carbocation. *J Am Chem Soc* 2000;122:1664–74.
- [48] Toteva MM, Richard JP. Structure– reactivity relationships for addition of sulfur nucleophiles to electrophilic carbon: resonance, polarization, and steric/ electrostatic effects. *J Am Chem Soc* 2000;122:11073–83.
- [49] Bai WJ, David JG, Feng ZG, Weaver MG, Wu KL, Pettus TRR. The domestication of ortho-quinone methides. *Acc Chem Res* 2014;47:3655–64.
- [50] Zhao Y-H, Li Y, Guo T, Tang Z, Xie W, Zhao G. Selective synthesis of pyrazolo[5,1-a]isoquinolines via 1,3-dipolar cycloaddition reaction. *Tetrahedron Lett* 2016;57:2257–61.
- [51] Zhao Y-H, Luo M, Li Y, Liu X, Tang Z, Deng K, Zhao G. Efficient synthesis of isoquinolines by AgNO<sub>3</sub>-catalyzed sequential imination–annulation of 2-alkynyl aldehydes with ammonium bicarbonate. *Chin. J Chem* 2016;34:857–60.
- [52] Zhao Y-H, Li Y, Luo M, Tang Z, Deng K. AgNO<sub>3</sub>-mediated cyclization/N-N bond cleavage reaction for the synthesis of 3-aryl isoquinolines. *Synlett* 2016;27:2597–600.
- [53] Zhao Y-H, Luo Y, Zhu Y, Wang H, Zhou H, Tan H, Zhou Z, Ma Y-C, Xie W, Tang Z. Synthesis of potential anticancer 1-(1H-indol-3-yl)-isoquinolines via AgNO<sub>3</sub>-mediated tandem reactions of 2-alkynylbenzaldehyde azines and indoles. *Synlett* 2018;29:773–8.
- [54] Tian M, Zheng G, Fan X, Li X. Rhodium (III)-Catalyzed redox-neutral synthesis of isoquinolinium salts via C–H activation of imines. *J Org Chem* 2018;83:6477–88.
- [55] Ye Z-S, Guo R-N, Cai X-F, Chen M-W, Shi L, Zhou Y-G. Enantioselective iridium-catalyzed hydrogenation of 1- and 3-substituted isoquinolinium salts. *Angew Chem Int Ed* 2013;52:3685–9.
- [56] Zhao Y-H, Luo Y, Wang H, Wei H, Guo T, Tan H, Yuan L, Zhang X-B. A novel ratiometric and reversible fluorescence probe with a large Stokes shift for Cu<sup>2+</sup> based on a new clamp-on unit. *Anal Chim Acta* 2019;1065:134–41.